The Study of Circumgalactic Medium with Quasar Pairs

ZHI-FU CHEN, HUAN-CHANG QIN, JIN-TING CAI, YU-TAO ZHOU, ZHE-GENG CHEN, TING-TING PANG, ZHI-WEN WANG

ABSTRACT

We have collected 10025 foreground-background quasar pairs with projected distances $d_p < 500\,$ kpc from the large quasar catalog of the SDSS DR16Q. We investigate the properties of the Mg II absorption lines with $W_r > 0.15\,$ Å around foreground quasars, including both the LOS (line-of-sights of foreground quasars) and transverse (TRA, perpendicular to the LOS) absorptions. Both the equivalent width (the correlation coefficient $\rho = -0.915\,$ and the probability $P < 10^{-4}\,$ of no correlation) and incident rate ($\rho = -0.964\,$ and $P < 10^{-6}$) of TRA Mg II absorption lines are obviously anti-correlated with projected distance. The incident rate of TRA Mg II absorption lines is obviously (> 4σ) greater than that of LOS Mg II absorption lines at projected distances $d_p < 200\,$ kpc, while the TRA and LOS Mg II both have similar (< 3σ) incident rates at scales $d_p > 200\,$ kpc. The anisotropic radiation from quasars would be the most possible interpretation for the anisotropic absorption around quasars. This could also indicate that the quasar radiation is not obviously impacting the gas halos of quasars at scales $d_p > 200\,$ kpc.

Keywords: galaxies: general —galaxies: halo — galaxies: active — quasars: absorption lines

1. INTRODUCTION

Since absorption lines were observed on quasar spectra, a great effort has been made to understand the link between absorbing gas and foreground galaxies approaching to the quasar sightline (e.g., Bahcall & Salpeter 1966; Bahcall & Spitzer 1969; Opher 1974; Roeser 1975; Burbidge et al. 1977; Bahcall 1978). The absorbing gas content is likely related to the global properties of galaxies. The number density of absorbers and star formation rate density of galaxies show similar evolution profile (e.g., Prochter et al. 2006; Matejek & Simcoe 2012; Cooksey et al. 2013; Chen 2013; Zhu & Ménard 2013; Madau & Dickinson 2014; Chen et al. 2015), implying that the star formation rate within galaxy would be an important factor giving rise to absorption line. A more positive evidence for the relationship between absorption line and star formation rate is that the Mg II with larger equivalent widths tend to host [OII] with stronger emission flux. (e.g., Ménard et al. 2011; Nestor et al. 2011; Shen & Ménard 2012; Joshi et al. 2018). The luminosity of a galaxy plays a role in the spatial distribution of gas in its dark matter halo (Tinker &

zhichenfu@126.com, hcqin@bsuc.edu.cn

Chen 2008), and the strength of absorption line is dominated by the amount of gas, therefore the properties of absorption lines are found to be related to the luminosity and stellar mass of galaxy (e.g., Chen & Tinker 2008; Chen et al. 2010a,b; Lovegrove & Simcoe 2011; Churchill et al. 2013; DeFelippis et al. 2021; Huang et al. 2021). Morphology, inclination, azimuthal angle with respect to the major axis of a galaxy, and environment of galaxies also influence the quantity of gas that the quasar sightline intercepts, therefore the connection between them and the properties of absorption lines are widely investigated(e.g., Kacprzak et al. 2007, 2011; Bordoloi et al. 2011; Cunnama et al. 2014; Barnes et al. 2014; Tumlinson et al. 2017; Lan & Mo 2018; Ho et al. 2020; Lee et al. 2021). In the last years, blind searches for galaxies associated with absorbers also revealed that the absorber's properties are related to the gravitational interactions in the group populations, galaxy's outflows, intergalactic medium accretions, star formation rates, and gas distributions within galaxy group (e.g., Fossati et al. 2019; Bielby et al. 2020; Dutta et al. 2020; Nielsen et al. 2020; Muzahid et al. 2021; Nielsen et al. 2022; Lofthouse et al. 2022). In addition, one absorber might be associated with multiple galaxies within a group as well (e.g., Bielby et al. 2020; Lofthouse et al. 2022).

The activity in nuclei is an important factor regulating the distribution and amount of galaxy gas. The

 $^{^2}$ School of Mathematics and Physics, Guangxi Minzu University, Nanning 530006, China

integral field units (IFU) is a good method to investigate the kinematic properties across the entire galaxies (e.g., Barrera-Ballesteros et al. 2014; Law et al. 2015; Jin et al. 2021; Zhou et al. 2022). Making full use of the absorption lines originated in gaseous halo of normal galaxies and imprinted in the spectra of background objects, considerable studies(e.g., Huang et al. 2016; Lan & Mo 2018; Ho et al. 2020; Anand et al. 2021; Huang et al. 2021) revealed that the absorption line properties related to the structure of gaseous halo, star formation activity, morphology, environment of the galaxy. Meanwhile over the last 20 years, noticeable attentions(e.g., Bowen et al. 2006; Hennawi et al. 2006; Farina et al. 2014; Johnson et al. 2015) are also paid to study the gaseous halo of the galaxy existing a quasar in its center with its absorptions to the background quasars, and uncovered that the gas extension, distribution, and content are related to the activities within the galaxy centre. It is widely accepted that the circumgalactic medium (CGM) surrounding quasar is a reservoir of enrich gas (e.g., Prochaska et al. 2013a; Johnson et al. 2015). The study of quasar CGMs is a good chance to investigate the surrounding environment and feedback of quasar. In the last decade, many works have also been focused on the emissions from CGMs (e.g., Hennawi & Prochaska 2013; Cantalupo et al. 2014; Martin et al. 2014, 2015; Hennawi et al. 2015; Borisova et al. 2016; Farina et al. 2017; Ginolfi et al. 2018; Arrigoni Battaia et al. 2018, 2019; Cai et al. 2019; Cantalupo et al. 2019; Drake et al. 2019; Farina et al. 2019; O'Sullivan et al. 2020; Guo et al. 2020; Burchett et al. 2021; Fossati et al. 2021). The investigations in emissions are redshift dependent and might spend a lot of exposure time of large-aperture telescopes, but a single exposure can image the entirety of the nebular emission. Although the detection of absorption features is limited to a single (or a few at max) location in the gas halo of a galaxy, it is redshift independent. Thus, the detections of emissions and absorptions from gas halo of the galaxy are the complementary approaches.

Absorption lines with redshifts close to quasar systemic redshifts ($z_{\rm abs}{\approx}z_{\rm em}$, associated absorption line) are likely formed in gaseous cloud physically associated with quasar themselves. Large samples(e.g., Shen & Ménard 2012; Chen et al. 2016; He et al. 2017; Chen et al. 2018a,b, 2020, 2022b) of associated absorption lines have been available through systematically analyzing the quasar spectra from the Sloan Digital Sky Survey (SDSS, York et al. 2000), which can often be used to comprehend the gas content of quasar systems along sightlines. The major shortcoming of associated absorption lines along quasar sightlines is that they can

not provide any information of gas content located on the transverse direction of quasars. If the sightline of a background luminous quasar passes through the vicinal medium of a foreground quasar, one can make use of the absorption features imprinted on the background quasar spectra to limit more comprehensively the gas content and environment surrounding the foreground quasar.

The supermassive black hole and powerful outflows/jets of quasars might significantly affect surrounding environments via strong feedbacks (e.g., Chen et al. 2022a; Zhu et al. 2022), leading to the properties of quasar CGMs substantially differ from those of normal galaxies. The strong radiation originated from quasar might photoionize, and even photoevaporate surrounding gas from tens kpc to a few Mpc (e.g., Wild et al. 2008; Tytler et al. 2009; Prochaska et al. 2014; Johnson et al. 2015; Jalan et al. 2019; He et al. 2022). In addition, the strong directional jet probably gives rise to anisotropic gas halo around quasar (e.g., Antonucci 1993; Elvis 2000; Hennawi & Prochaska 2007; Farina et al. 2014; Almeyda et al. 2017; Jalan et al. 2019). Along the sightlines of quasars, the powerful outflows/jets likely over ionize the gas medium with low ionization states and close to quasar central regions. While along the transverse direction, the gas medium is likely much less illuminated by the radiation from guasars and maintained low ionization state. These would be the most possible explanation to the proximity effect along the quasar's sightline and inverse proximity effect along transverse directions of quasars (e.g., Hennawi & Prochaska 2007; Jalan et al. 2019)¹. Here, the inverse proximity effect indicates that the number of absorption lines is increased with decreasing distance from quasar central regions.

Recently, as more and more quasars are discovered, the technique that quasars probe quasars is widely used to investigate the surrounding gas of quasars with absorption lines (e.g., Bowen et al. 2006; Hennawi et al. 2006; Hennawi & Prochaska 2007; Tytler et al. 2009; Farina et al. 2013; Hennawi & Prochaska 2013; Prochaska et al. 2013b; Farina et al. 2014; Prochaska et al. 2014; Sandrinelli et al. 2014; Johnson et al. 2015; Kacprzak et al. 2015; Landoni et al. 2016). It is almost without exception that all the neutral hydrogen Ly α , and metal

¹ In the vicinity of quasars, one expects that the amount of absorption lines should be increased with decreasing distance from quasar central regions. However, the strong radiation from quasars reduces the detectable absorption lines with lower ionization state as the absorption redshifts closer to the emission redshifts of the quasars. This phenomenon is commonly called as proximity effect (e.g., Carswell et al. 1982; Srianand & Khare 1996; Prochaska et al. 2013b).

C II, C IV and Mg II absorptions exhibit an excessive incidence over cosmic average on transverse direction, and the incident rate of absorptions on transverse direction is inversely proportional to the projected distance from foreground quasars. In this paper, making use of the final quasar catalog from the SDSS, we construct a large sample of foreground-background quasar pairs to statistically analyze the properties of Mg II $\lambda\lambda 2796,2803$ absorbing gas around foreground quasars, including the absorptions in the line-of-sight (LOS absorptions) and transverse (TRA absorptions) directions of foreground quasars. Making use of the LOS and TRA Mg II absorption lines, ones can examine more thoroughly the gas environment surrounding quasars.

Throughout this work, we assume a flat Λ CDM cosmology with $\Omega_m = 0.3$, $\Omega_{\Lambda} = 0.7$, and $h_0 = 0.7$.

2. SAMPLE SELECTION

The SDSS is an ambitious project to image the sky using a dedicated 2.5 m wide-field telescope (Gunn et al. 2006) located at Apache Point Observatory in New Mexico, United States. During the first and second stages (Abazajian et al. 2009, SDSS-I/II, from 2000 — 2008;), the SDSS obtained quasar spectra in a coverage wavelength from 3800 Å to 9200 Å with $R \equiv \lambda/\Delta\lambda \approx 2000$. During the third and fourth stages (SDSS-III/IV, from 2008 — 2020; Smee et al. 2013; Dawson et al. 2013, 2016), the SDSS gathered quasar spectra in a coverage wavelength from 3600 Å to 10500 Å at a resolution of $R \approx 1300 \sim 2500$. The Sixteenth Data Release is the final dataset for the SDSS-IV quasar catalog(DR16Q; Lyke et al. 2020), which includes 750,414 quasars that are accumulated from SDSS-I to SDSS-IV. Using the quasar spectra from DR16Q, we construct a large sample of quasar pairs to investigate the properties of Mg II $\lambda\lambda 2796,2803$ absorption lines around foreground quasars. We select quasars from DR16Q with following criteria.

- 1. The projected distance of quasar pairs at fore-ground quasar redshifts are limited to $d_p < 500$ kpc. Note that the 500 kpc is a conservative value. The halo size of a massive galaxy might be less than 200-300 kpc, and the gas located at a distance > 500 kpc from the quasar center region is likely related to the halo of satellite galaxy (e.g., Zhu et al. 2014)
- 2. Narrow absorption lines are often confused by Ly α forest absorptions if they fall into the spectral region with $(1 + z_{\rm em}) \times \lambda_{\rm Ly\alpha} > (1 + z_{\rm abs}) \times \lambda_{abs}$, where the $\lambda_{\rm Ly\alpha}$ and $\lambda_{\rm abs}$ are rest-frame wavelengths of the Ly α emission line and detected

absorption line, respectively. The absorptions of N V $\lambda\lambda 1238,1242$ are often presented in the red wings of Ly α emission lines, which would lead to misidentifications Mg II $\lambda\lambda 2796,2803$ absorption doublets. Therefore, we conservatively cut off parent sample to quasars with $(1+z_{\rm em}(fg))\times 2800 \mbox{Å} \geq (1+z_{\rm em}(bg))\times 1300 \mbox{Å}$, where $z_{\rm em}(fg)$ and $z_{\rm em}(bg)$ are systematical redshifts of foreground and background quasars, respectively.

- 3. Accounting for the rest-frame wavelength of Mg II absorption lines and the coverage wavelengths of the SDSS spectra, we only consider the quasars with $z_{em} > 0.4$. In addition, in order to avoid the contamination from outflows of background quasars, the differences between the redshifts of foreground and background quasars $\Delta v(z_{em}(fg), z_{em}(bg)) > 6000 \text{ km s}^{-1}$.
- 4. The LOS Mg II absorption lines are detected in the spectral data around the Mg II emission lines of foreground quasars. Thus, we only select the foreground quasars with median signal-to-noise ratio S/N >3 within the spectral regions of ± 6000 km s $^{-1}$ around Mg II emission lines.
- 5. The TRA Mg II absorption lines are detected in the background quasar spectra. Thus, we also limit the background quasars with median signal-to-noise ratio S/N > 3 within the spectral regions of $\pm 6000~{\rm km\,s^{-1}}$ around foreground quasar redshifts.

Above limits yield a sample of 10025 foreground-background quasar pairs. Using bolometric luminosity correction factor (e.g., Shen et al. 2011), we also compute the bolometric luminosity of the quasar from the flux density of the pseudo-continuum fitting at 3000 Å, or 1350 Å when the spectral data at 3000 Å are not available for high redshift quasars. The parameters of quasar pairs are listed in Table 1 and 2.

2.1. Quasar redshifts

The blueshifted and/or asymmetrical profiles of emission lines could bias quasar redshifts of the SDSS pipeline, which are able to result in an uncertainty from 100 km s $^{-1}$ to 3000 km s $^{-1}$ (e.g., Hewett & Wild 2010; Shen et al. 2011; Chen et al. 2019). The large uncertainty could give rise to an absorber detected at the quasar redshift absolutely outside galaxy halo. Therefore, the more accurate quasar redshifts are required to probe the environmental gas surrounding quasars via absorption lines with $z_{\rm abs}\approx z_{\rm em}$. Narrow emission line often provides quasar redshift with higher accuracy than

Table 1. The properties of the quasar pairs and the LOS Mg II absorption lines

Pair ID	SDSS name foreground	PlateID	MJD	FiberID		$LogL_{bol}$ $erg s^{-1}$		$z_{ m abs}$	$W_{\mathrm{r}}^{\lambda 279}$ Å	$^6\sigma_{W^{\lambda_2796}_{ m r}}$ Å	$W_{ m r}^{\lambda 2803}$ Å	$^3\sigma_{W^{\lambda_{2803}}_{ m r}}$ Å	SDSS name
1	154530.23+484608.9	8429	57893	8 896	0.4009	46.304	459.0	-	_	0.02	-	0.02	154535.84+484713.6
2	081107.57+342940.8	9355	57814	84	0.4000	44.609	422.1	-	-	0.15	-	0.15	081104.05 + 342835.5
3	075051.72 + 245409.3	928	52578	3 232	0.4003	46.174	475.0	-	-	0.04	-	0.04	075046.78 + 245311.9
4	114436.33+464232.9	1444	53054	103	0.4005	45.399	401.6	-	-	0.12	-	0.12	$114429.71\!+\!464202.6$
5	104859.47+313326.1	10472	58159	936	0.4016	44.944	274.8	-	-	0.09	-	0.09	104903.42 + 313318.3
6	094059.64+491618.3	7292	56709	446	0.4014	44.518	440.8	-	-	0.25	-	0.25	094105.87 + 491523.7
7	081931.20+334837.5	9358	57749	212	0.4021	46.243	484.4	-	-	0.02	-	0.02	081928.29 + 334959.7
8	083026.01+534834.0	7277	56748	350	0.4030	44.501	450.7	-	-	0.26	-	0.26	083021.29 + 534721.8
9	221132.77+241955.4	7643	57302	356	0.4031	44.751	494.4	-	-	0.16	-	0.16	221127.39 + 242049.9
10	234252.37-003915.3	9209	57686	655	0.4049	45.172	481.6	-	-	0.06	-	0.06	234256.67-003814.0
11	013457.91+002738.2	4230	55483	8 804	0.4048	44.394	422.00	0.4054	0.98	0.17	1.25	0.41	013502.28 + 002656.0

Note — Symbols "-" represent the spectra without detected Mg II absorption lines. Only the equivalent width of 1σ upper limit is provided for the spectra without detected Mg II absorption lines.

Table 2. The background quasars with TRA Mg $\,$ II absorption lines

Pair ID	SDSS name	PlateID	MJD	FiberID	$z_{ m em}$	$d_{ m p}$	$z_{ m abs}$	$W_{\mathrm{r}}^{\lambda2796}$	$\sigma_{W^{\lambda_{2796}}_{\mathrm{r}}}$	$W_{\mathrm{r}}^{\lambda2803}$	$\sigma_{W_{ m r}^{\lambda 2803}}$
						kpc		Å	Å	Å	Å
1	154535.84 + 484713.6	812	52352	360	1.4093	459.0	-	-	0.27	-	0.27
2	081104.05 + 342835.5	9355	57814	88	1.7466	422.1	-	-	0.27	-	0.27
3	075046.78 + 245311.9	11104	58436	142	1.1430	475.0	-	-	0.26	-	0.26
4	114429.71 + 464202.6	7401	56808	654	1.5080	401.6	-	-	0.30	-	0.30
5	104903.42 + 313318.3	6445	56366	604	0.8480	274.8	-	-	0.09	-	0.09
6	094105.87 + 491523.7	7292	56709	450	1.7984	440.8	-	-	0.26	-	0.26
7	081928.29 + 334959.7	3759	55236	190	0.7810	484.4	-	-	0.13	-	0.13
8	083021.29 + 534721.8	7277	56748	346	1.5672	450.7	-	-	0.17	-	0.17
9	221127.39 + 242049.9	7643	57302	354	1.1602	494.4	-	-	0.16	-	0.16
10	234256.67-003814.0	9209	57686	659	1.8035	481.6	-	-	0.26	-	0.26
11	013502.28 + 002656.0	697	52226	621	1.4232	422.0	-	-	0.17	-	0.17
12	131144.26 + 420411.3	6620	56368	312	0.6550	450.2	-	-	0.11	-	0.11
13	145310.47 + 420034.8	1397	53119	576	0.8046	261.3	-	-	0.17	-	0.17
14	151928.77 + 573807.2	612	52079	548	1.4930	420.0	-	-	0.12	-	0.12
15	091517.07 + 332155.7	10242	58161	573	1.8943	363.4	-	-	0.16	-	0.16
16	075204.01 + 345711.3	9354	57806	296	1.7245	451.8	-	-	0.12	-	0.12
17	100605.21 + 351159.9	4637	55616	130	1.4750	352.8	-	-	0.22	-	0.22
18	025257.22-072217.4	457	51901	429	1.4488	344.7	-	-	0.21	-	0.21
19	090558.02 + 411725.7	4605	55971	830	0.6038	414.1	-	-	0.16	-	0.16
20	085850.21 + 514655.1	5155	55946	174	2.0286	303.0	-	-	0.15	-	0.15
21	$014729.24\!+\!002000.7$	7843	56902	934	1.5188	254.1	0.4053	1.75	0.50	0.65	0.24

Note — Symbols "-" represent the spectra without detected Mg II absorption lines. Only the equivalent width of 1σ upper limit is provided for the spectra without detected Mg II absorption lines.

broad emission line does. And also, Shen 2016 suggests an uncertainty of about 200 km s $^{-1}$ when quasar redshifts are determined from Mg II $\lambda2798$ emission lines relative to those measured from [O III] $\lambda5007$ emission lines. This small uncertainty suggests that the Mg II emission line can better determine quasar redshift than the Ly α , C III], and C IV emission lines do (e.g. Hewett & Wild 2010; Shen et al. 2011). Therefore, we determine quasar redshifts in the following order.

- 1. We adopt the redshifts of Hewett & Wild (2010) ² for quasars included in the SDSS DR7Q, who have improved the redshifts for the SDSS-I/II quasars using a cross-correlation method.
- 2. When narrow [O II] or [O III] emission lines are available by the SDSS spectra, we determine quasar redshifts by fitting these emission lines with Gaussian function(s).
- 3. Using the template of Hewett & Wild (2010), we measure the redshifts from Mg II or C III] emission lines when available.

We include a velocity correction of 200 km s⁻¹ (Shen 2016) for the systemic redshifts determined from the Mg II emission line, so that the redshifts are more consistent with those determined from the [O III] emission line (Hewett & Wild 2010). Figure 1 shows the redshift distributions of background quasars with black solid-line and foreground quasars with red dash-line. The red dash-line exhibits a dip at $z_{\rm em} \sim 1.1$, which is caused by the decreasing sensitivity during the split of the red and blue spectrographs³. The projected distances of quasar pairs are displayed in Figure 2.

3. ABSORPTION LINE MEASUREMENTS

The Mg II absorption lines imprinted in the quasar spectra can be originated in intervening galaxies that are far beyond the gravitational bound of quasars, and the gas clouds within quasar's outflows, host galaxies, halos, and galaxy clusters. Using large samples of LOS absorption lines, previous works(e.g., Chen & Pan 2017; Chen et al. 2018a) claims that: (1) the relative velocity of $v_{\rm r} < 6000~{\rm km\,s^{-1}}$ with respect to quasar systemic redshifts is a safe boundary to constrain a vast majority of Mg II absorption lines from quasar's outflows, host galaxies, halos, and galaxy clusters; while (2) the velocity range of $\pm 1500~{\rm km\,s^{-1}}$ can well constrain the Mg II absorption lines formed within quasar's host

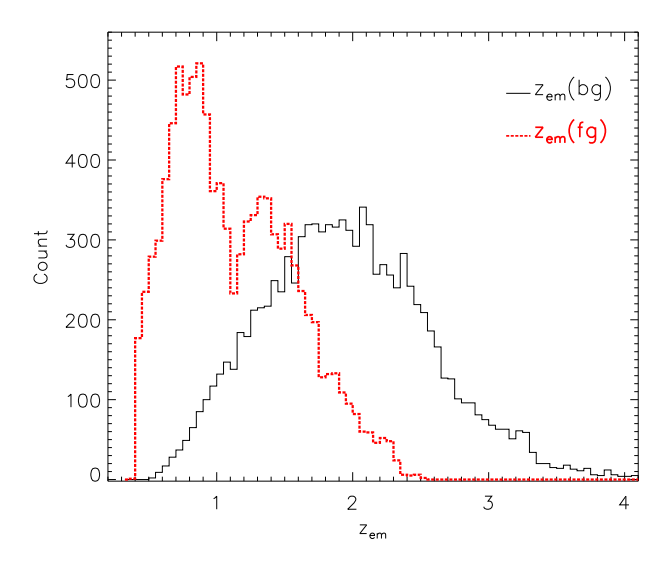


Figure 1. Redshift distributions. Black solid-line and red dash-line are for background and foreground quasars, respectively.

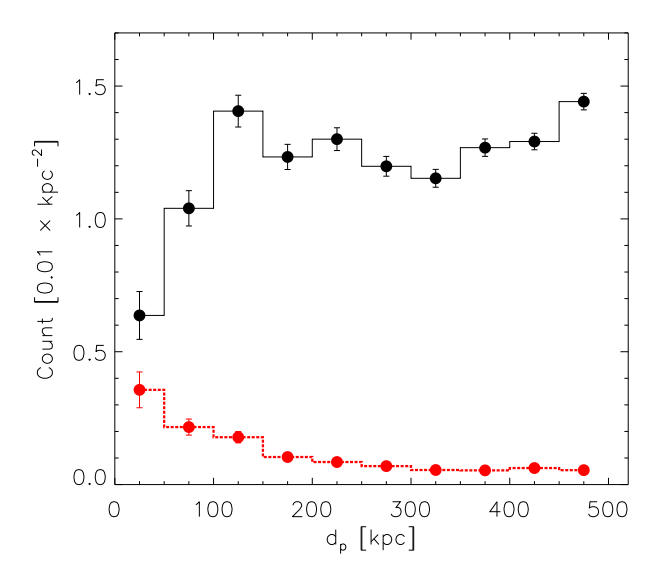


Figure 2. Distributions of projected distances of quasar pairs, which have been normalized by the circular area spanned by each annulus. Black symbols are for all the quasar pairs, and red symbols are only for quasar pairs with detected TRA Mg II absorption lines in the background quasar spectra.

galaxies, halos, and galaxy clusters. We also note from Chen et al. (2018a) that the fraction of the intervening Mg II absorption lines is similar to that of the associated ones in the velocity range of $v_{\rm r}=1500-6000$ km s⁻¹. In other words, the associated Mg II absorption lines are significantly contaminated by the intervening ones in the velocity range of $v_{\rm r}=1500-6000$ km s⁻¹.

 $^{^2 \} http://das.sdss.org/va/Hewett_Wild_dr7qso_newz/$

³ http://www.sdss.org/dr7/instruments/spectrographs

In addition, the associated Mg II absorption lines with $v_{\rm r} = 1500 - 6000 \,\,\mathrm{km}\,\mathrm{s}^{-1}$ are dominated by quasar's outflows. This work aims to investigate the properties of gas clouds within quasar's host galaxies and halos, making use of the Mg II absorption lines with $z_{\rm abs} \approx$ $z_{\rm em}(fg)$. Therefore, in both the foreground and background quasar spectra, we search for Mg II absorption lines within the spectral regions of $\pm 1500 \text{ km s}^{-1}$ around Mg II emission lines of the foreground quasars. Note that, if the spectral regions used to search for Mg II absorption lines are located within a broad absorption feature, we directly exclude the spectra from our parent sample. Figure 3 shows the SDSS spectra and images of two pairs of quasars. The shaded yellow regions label the wavelength ranges used to search for associated Mg II absorption lines of foreground quasars.

We firstly masked out the strong absorption lines around the spectral regions used to searched for Mg II absorption lines. Then cubic spline (for underlying continuum) plus Gaussian functions (for emission line features) are invoked to derive the pseudo-continuum fitting (see the red-solid lines shown in Figure 3), which is used to normalize spectral flux (flux divided by the pseudo-continuum fitting) and flux uncertainty (flux uncertainty divided by the pseudo-continuum fitting) (e.g., Chen et al. 2015, 2018a). Here the spline is extrapolated over the continuum underneath the emission line. We search for and visually inspect the Mg II absorption doublets on the normalized spectra, and model each doublet with a pair of Gaussian functions. The integration of the Gaussian modeling gives absorption equivalent width at rest frame (W_r) . The error of the W_r (σ_w) is derived by directly integrating the normalized flux uncertainty within $\pm 3\sigma$ widths, where the σ is given by the Gaussian modeling. We only keep the Mg II absorption lines with $W_{\rm r}^{\lambda2796} \geq 2\sigma_{\rm w}$ and $W_{\rm r}^{\lambda2796} \geq 0.15$ Å. For the spectra without detected Mg II absorption lines, we estimate the $\sigma_{\rm w}$ within 200 km s⁻¹, which are taken as the upper limits of the $W_{\rm r}$ as well. The absorption parameters of the detected Mg II absorption lines are listed in 1 and

4. TRANSVERSE ABSORPTION LINES

In the large sample of 10025 foreground-background quasar pairs, we find that there are 598 background quasars with detected TRA Mg II absorption lines that are associated to foreground quasars. Figure 4 shows the velocities of the TRA Mg II absorption lines relative

to foreground quasar systemic redshifts 4 . About 90% of the TRA Mg II absorption lines are located within $|v_r| < 600~{\rm km\,s^{-1}}$ (0.002c). The projected distances of the TRA Mg II absorption lines are also displayed with red dash-line in Figure 2. It is clearly seen that the TRA Mg II absorption lines are more likely to be detected in the spectra of background quasars with smaller projected distances. In addition, the projected distances of the TRA Mg II absorbing clouds are from 20 kpc to 500 kpc, which implies that the TRA Mg II absorption lines would be mainly dominated by the halos of foreground quasar host. Of course, neighbouring halos of quasars might also contribute to the TRA Mg II absorption lines with $d_{\rm p} > 300~{\rm kpc}$ (e.g., Zhu et al. 2014).

The velocity widths of Mg II absorption lines provide dynamical information of absorbing clouds around quasar host galaxies. For the luminous red galaxies (LRGs), Zhu et al. (2014) revealed that the velocity widths of Mg II absorption lines with $\sigma < 300 \text{ km s}^{-1}$ on scales $d_p < 300\,$ kpc, where the σ is the velocity dispersion of gas cloud measured from the Gaussian fits of absorption lines, mainly reflect the motion of gas clouds within halos of LRGs host, while the velocity widths of Mg II absorption lines with $\sigma > 300 \text{ km s}^{-1}$ on scales $d_p > 600$ kpc are related to the motion of gas clouds of the neighbouring halos of the LRGs. In Figure 5, we show the velocity dispersions measured from the TRA Mg II absorption lines. It can be seen that the velocity dispersions of the Mg II gas clouds are less than 250 ${\rm km\,s^{-1}}$, and mainly constrained within a velocity range of $60 - 150 \text{ km s}^{-1}$ (about 87% of the TRA Mg II absorption lines). Meanwhile, velocity dispersions are not obviously changed with projected distances. The velocity dispersion with small/mild values and not changed with projected distances, imply again that the TRA Mg II absorption lines would be mainly reflect the properties of gas clouds within the halos of quasar host, but not within the neighbouring halos of quasars.

For the background quasars, we shift them to rest frame of the foreground quasars or the Mg II absorbers when the TRA Mg II absorption lines are available, and then produce median composite spectra. We measure the equivalent widths of Mg II absorption lines in composite spectra. The results are shown in Figure 6 and listed in Table 3. The Mg II equivalent width is decreased with increasing projected distance before d < 400 kpc. We invoke the Spearman's correlation

 $^{^4}$ $\upsilon_r = \frac{(1+z_{\rm abs})^2 - (1+z_{\rm em})^2}{(1+z_{\rm abs})^2 + (1+z_{\rm em})^2},$ where $z_{\rm abs}$ is the absorption line redshift determined from MgII $\lambda 2796,$ and $z_{\rm em}$ is the systemic redshift of foreground quasar.

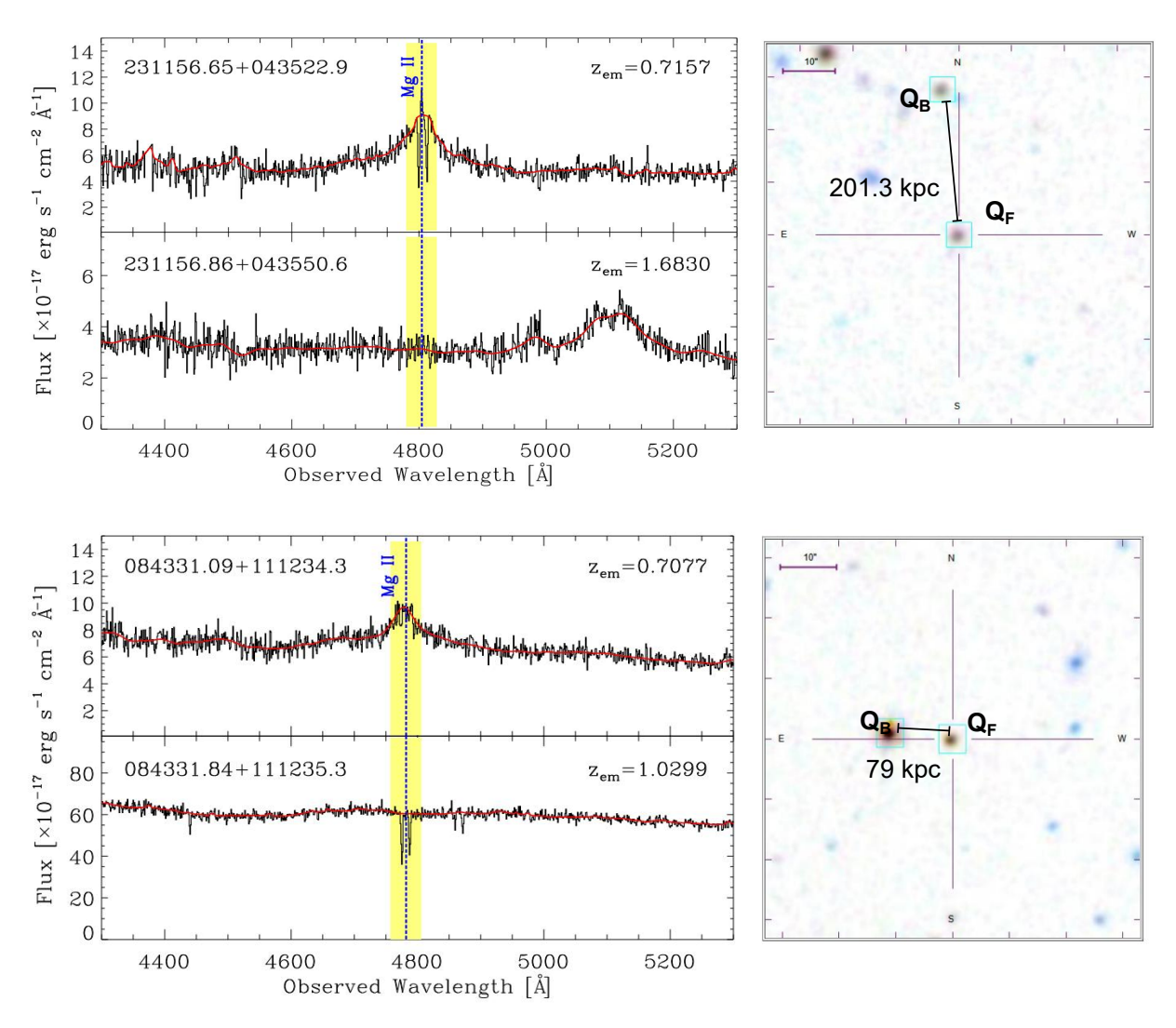


Figure 3. Examples of two pairs of quasars. Left panels show the SDSS spectra of quasars. Red solid-lines are the fitting pseudo-continuum, blue dash-lines label the positions of Mg II emission lines of foreground quasars, and the shaded yellow regions label the spectral regions used to search for associated Mg II absorption lines of foreground quasars. For the quasar pair of J231156.65 + 043522.9 and J231156.86 + 043550.6, having a projected distance of $d_{\rm p}=201.3$ kpc, an obvious Mg II absorption line is displayed in the spectra of foreground quasar, but not in the spectra of background quasar. For the quasar pair of J084331.09 + 111234.3 and J084331.84 + 111235.3, having a projected distance of $d_{\rm p}=79$ kpc, an obvious Mg II absorption line is displayed in the spectra of background quasar, but not in the spectra of foreground quasar. Right panels show the SDSS images of the fields around the foreground quasars. The background and foreground quasars are labelled as $Q_{\rm B}$ and $Q_{\rm F}$, respectively. The purple lines at the top left of images are 10 arcsec in length.

test to the relationship between the Mg II equivalent widths and projected distances, which yields a correlation coefficient $\rho=-0.915$ and a probability $P<10^{-4}$ of no correlation. This decreased trend is similar to previous results and also hosted by other transitions, such as C IV, C II, Si IV absorption lines, no matter what type of galaxies these absorbing clouds surround (e.g., Steidel et al. 2010; Prochaska et al. 2014; Zhu et al. 2014; Johnson et al. 2015; Landoni et al. 2016; Lan & Mo 2018).

Recently, using background quasars, Lan & Mo (2018) investigated the properties of Mg II absorption lines

around emission line galaxies (ELGs) and luminous red galaxies (LRGs). In Figure 6, we also display the results of Lan & Mo (2018) with blue or red triangles. The Mg II absorption strengths are stronger around ELGs than around quasars on scales smaller than 50 kpc. This might be due to some of the Mg II absorption lines around ELGs associated to the outflows of ELGs on small scales, while the TRA Mg II absorption lines of quasars are not related to outflows, since the the vast majority of quasar sightlines would be close to the axis of accretion disk. We also note that the Mg II absorp-

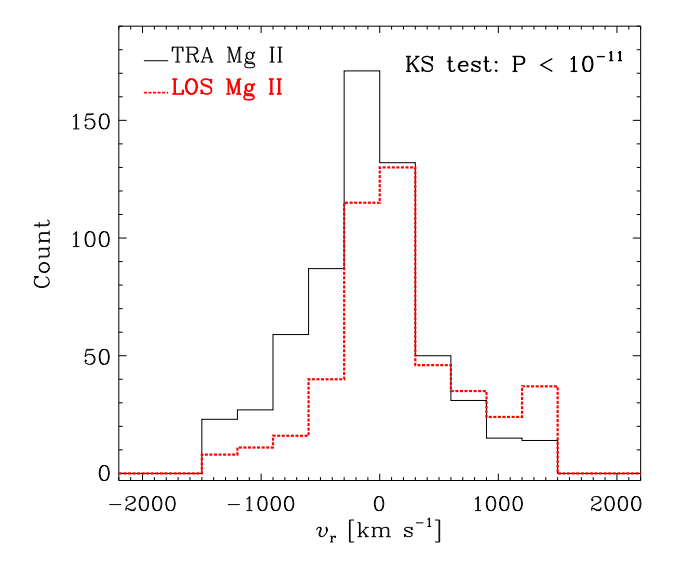
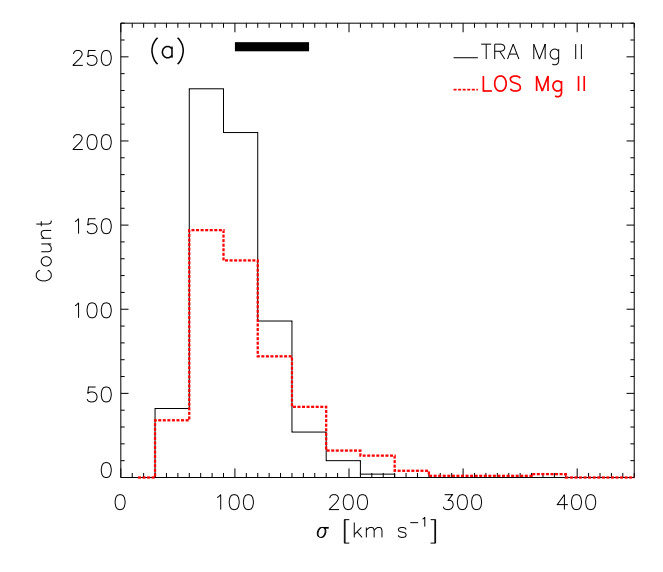


Figure 4. Velocity distributions of Mg II absorption lines relative to foreground quasar systemic redshifts. Black solid-line and red dash-line are for the TRA and LOS Mg II absorption lines, respectively.

tion strengths are stronger around quasars than around LRGs on all scales, and than around ELGs on scales greater than 100 kpc. The ELGs and LRGs used by Lan & Mo (2018) have redshift ranges of $z \approx 0.4 - 1.5$, and $z \approx 0.4$ — 0.8, respectively. These redshift ranges are obviously smaller than that $(z \approx 0.4 - 2.6)$ of foreground quasars used in this paper. Here we limit our quasar pair sample with redshifts of foreground quasars $z_{\rm em}(fg) < 1.5$ and $z_{\rm em}(fg) < 0.8$, respectively. The results are displayed with green and orange squares in Figure 6, respectively. It is clearly seen that the discrepancies between quasars and ELGs or LRGs are not caused by redshifts. In order to check the influence from quasar radiations, we divide our quasar pair sample into two subsamples, namely, the subsamples of quasars with lower and higher luminosities, respectively. The results are also shown in Figure 6, which suggests that the Mg II equivalent width of the quasars with higher luminosities would be slightly greater than that of the quasars with lower luminosities.

5. LINE-OF-SIGHT ABSORPTION LINES

Absorption features detected in foreground quasar spectra with $z_{\rm abs} \approx z_{\rm em}$ are mainly formed within quasar's outflows/winds, host galaxies, halos, and galaxy clusters. Broad absorption lines (BALs) with line width larger than 2000 km s⁻¹, and mini-BALs with line width larger than a few hundreds km s⁻¹ and less than 2000 km s⁻¹ are usually considered to be associated to quasar's outflows/winds. Meanwhile, we note that for



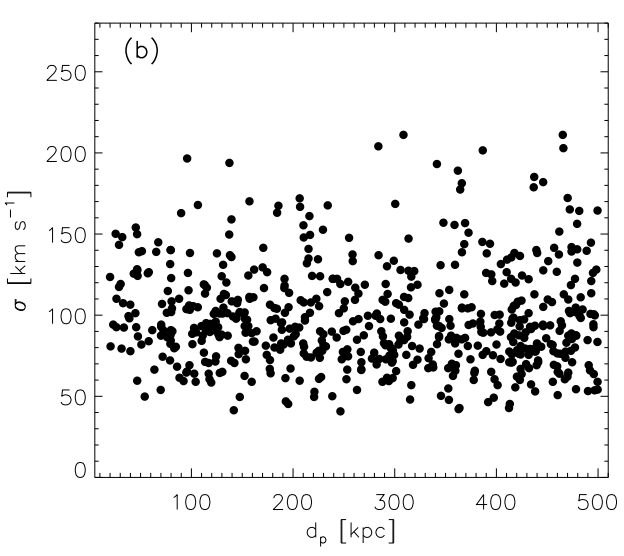


Figure 5. Panel (a): Velocity dispersions of gas clouds traced by Mg II absorption lines. Black solid-line and red dash-line are for the TRA and LOS Mg II absorption lines, respectively. The thick horizontal line is for the mean uncertainty of line widths, accounting for the typical spectral resolution of the SDSS/BOSS. Panel (b): Velocity dispersions of gas clouds traced by TRA Mg II absorption lines as a function of projected distances.

LRGs, the line width is less than 400 km s⁻¹ for the Mg II absorption lines formed within the gas clouds with projected distances less 1 Mpc (e.g., Zhu et al. 2014). In this work, we limit the TRA Mg II absorption lines with $d_{\rm p} < 500$ kpc and mainly focus on the absorption lines formed within the gas clouds of quasar's host galaxies and halos. Therefore, we only retain the LOS Mg II absorption lines with line width less than 500 km s⁻¹. In the large sample of 10025 foreground-background quasar

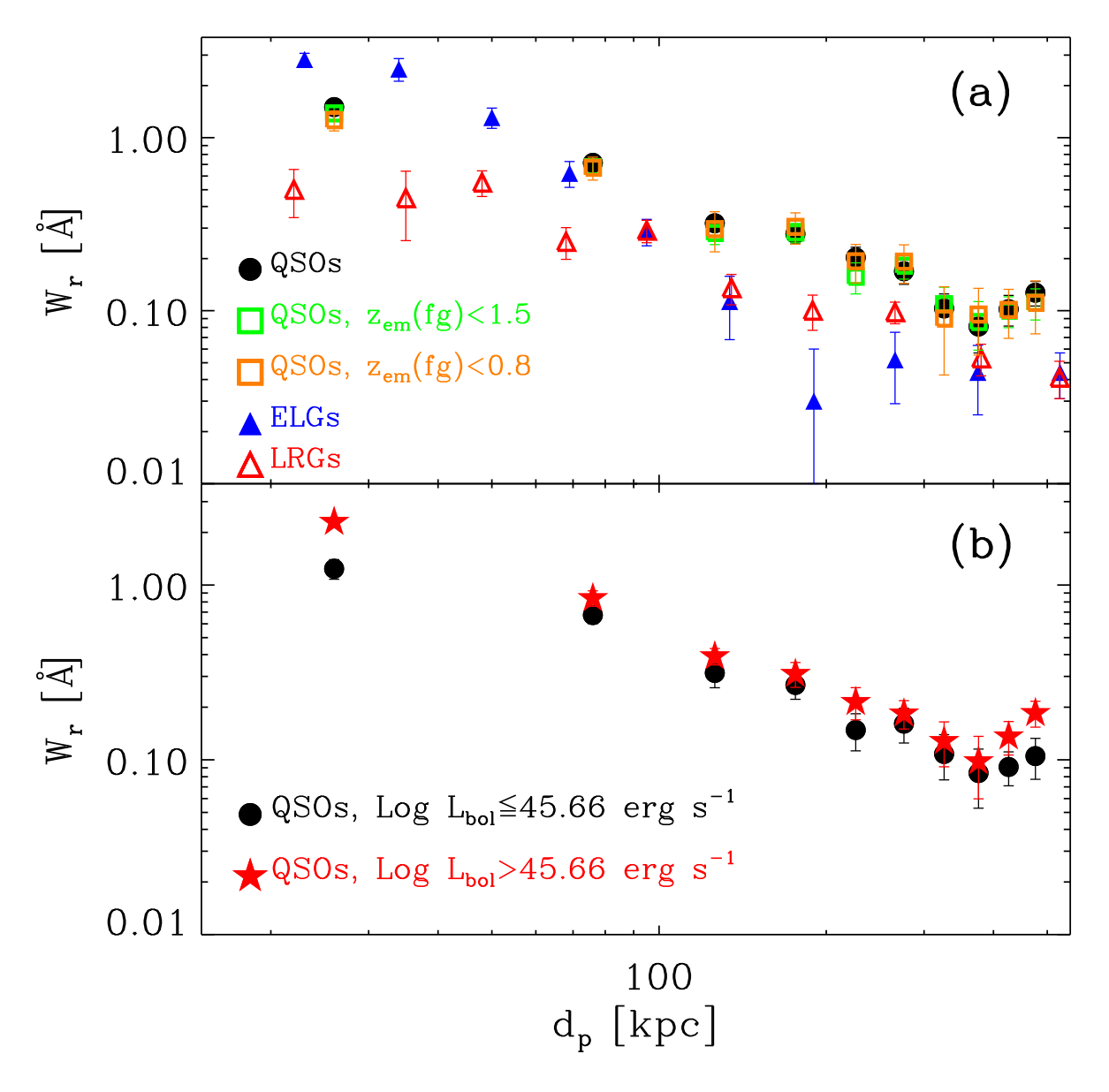


Figure 6. Mg II rest equivalent width, the sum of MgII $\lambda 2796$ and MgII $\lambda 2803$ lines, as a function of projected distance for the TRA absorption lines. Panel (a): Black filled circles are for all the quasar pairs; green and orange unfilled squares are for the quasar pairs whose foreground quasars have $z_{em}(fg) < 1.5$ and $z_{em}(fg) < 0.8$, respectively; blue filled triangles and red unfilled triangles are for the TRA Mg II absorption lines around the emission line galaxies and luminous red galaxies from Lan & Mo (2018), respectively. Panel (b): Black circles are for the quasar pairs whose foreground quasars have $LogL_{bol} \leq 45.66$ erg s⁻¹, and the red stars are for the quasar pairs whose foreground quasars have $LogL_{bol} > 45.66$ erg s⁻¹, where the $LogL_{bol} = 45.66$ erg s⁻¹ is the median value of the bolometric luminosities of foreground quasars.

pairs, we find that there are 454 foreground quasars with detected LOS Mg $\,$ II absorption lines.

The velocity dispersions measured from the LOS Mg II absorption lines are shown with red dash-line in Figure 5. In addition to 4 LOS Mg II absorption lines, all the LOS Mg II absorption lines yield a velocity dispersion $\sigma < 300 \text{ km s}^{-1}$. About 75% of the LOS Mg II absorption lines are also constrained within a velocity range of $60 - 150 \text{ km s}^{-1}$, which implies that most of the

LOS Mg II gas clouds could be gravitationally bounded by quasar halos.

The velocities of LOS Mg II absorption lines relative to foreground quasar systemic redshifts are shown with red dash-line in Figure 4. About 79% of the LOS Mg II absorption lines are located within $|v_r| < 600 \text{ km s}^{-1}$. We perform the Kolmogorov-Smirnov (KS) test to the velocity distributions of the TRA and LOS Mg II, which yields a probability of $P < 10^{-11}$. This small probability

Table 3. The Mg $\,$ II equivalent widths measured from composite spectra

d_p bin kpc	$N_{ m pair}$	$W_{ m r}^{\lambda2796}$ Å	$W_{ m r}^{\lambda2803}$ Å
(0,50]	51	0.855 ± 0.084	0.647 ± 0.059
(50,100]	244	$0.417 {\pm} 0.044$	0.298 ± 0.037
(100,150]	552	$0.185{\pm}0.027$	0.135 ± 0.019
(150,200]	678	$0.147{\pm}0.027$	$0.131 {\pm} 0.022$
(200,250]	915	$0.106 {\pm} 0.023$	0.097 ± 0.019
(250,300]	1033	$0.097{\pm}0.021$	0.072 ± 0.017
(300,350]	1176	$0.056{\pm}0.015$	$0.047 {\pm} 0.016$
(350,400]	1491	$0.049 {\pm} 0.017$	$0.032 {\pm} 0.017$
(400, 450]	1722	$0.050 {\pm} 0.015$	$0.052 {\pm} 0.014$
(450,500]	2149	$0.068 {\pm} 0.016$	$0.059 {\pm} 0.013$

suggests that the velocities of the TRA Mg II are obviously different from those of the LOS ones. As a whole, the TRA and LOS Mg II absorption lines have mean velocities of $v_r = -116 \text{ km s}^{-1}$ and 160 km s^{-1} , when compared to quasar systemic redshifts. This implies that the TRA Mg II are slightly redshifted and the LOS ones are slightly blueredshifted relative to quasar systems. Lau et al. (2018) also claimed that the TRA absorption lines exhibit a small redshift relative to quasar systems. Both the redshifted TRA and blueshifted LOS absorption lines imply that the absorbing gas is on average dominated by galaxy's outflows. While, the small values of redshift (-116 km s⁻¹) and blueshift (160 km s⁻¹) can be compared to the uncertainty of quasar systemic redshits. Therefore, here we can not further investigate the intrinsic origins of the TRA and LOS Mg II with present data.

6. INCIDENT RATE OF Mg II ABSORPTION LINES

We define the incident rate of Mg II absorption lines at different projected distance as follows:

$$f_c = \frac{N_{\rm abs}}{N_{\rm QSO}},\tag{1}$$

where, at a given range of projected distance, $N_{\rm abs}$ represents the number of detected Mg II absorption lines (See Section 3 for the limits of detected absorbers), and $N_{\rm QSO}$ represents the number of quasars used to search for corresponding absorption lines. The error of f_c can be derived from the binomial statistics. In this section, we statistically analyze the incident rates of LOS and TRA Mg II absorption lines, respectively.

For transverse absorptions, we calculate f_c with Equation (1) in several bins of projected distance, here $N_{\rm abs}$

is the number of detected TRA absorbers, and $N_{\rm QSO}$ is the number of background quasars used to search for TRA Mg II absorption lines. The results are listed in Table 4.

The distance between the LOS absorbing cloud and quasar central region is a mystery, so we have no knowledge of the relationship between the f_c of the LOS Mg II absorption line and distance. While, we still estimate the f_c of LOS Mg II absorption lines with Equation (1), where $N_{\rm abs}$ represents the number of detected LOS Mg II absorption lines, and $N_{\rm QSO}$ represents the number of foreground quasar used to search for LOS Mg II absorption lines. In this way, the derived f_c is not the function of distance, and should be a constant.

In panel (a) of Figure 7, we show the derived f_c as a function of projected distance. It is clearly seen that the incident rate of the TRA absorption lines is decreased quickly with increasing projected distance. We invoke the Spearman's correlation test to the relationship between the f_c and projected distances, which yields a correlation coefficient $\rho = -0.964$ and a probability $P < 10^{-6}$ of no correlation. The decreasing tendency is consistent with previous results (e.g., Farina et al. 2014; Prochaska et al. 2014; Johnson et al. 2015). It is interesting that the f_c of TRA Mg II absorption lines is significantly (> 4σ) higher than that of LOS absorption lines on scales smaller than 200 kpc, while the TRA and LOS Mg II have similar (within 3σ) incidences on larger scales. This could be an indication that the guasar radiation is not significantly impacting the gas halos of quasars at scales $d_p > 200$ kpc. On small scales, significant difference in the incident rates between TRA and LOS Mg II absorption lines is likely related to the anisotropic radiation originated from quasars (e.g., Prochaska et al. 2013b; Lau et al. 2016, 2018; Jalan et al. 2019). Quasar's outflows/jets might inject significant energy into surrounding environment, through kinetic feedback and/or radiative pressure. Therefore, the powerful outflows/jets of quasars would over ionize the medium with lower ionization state, which is also the most possible interpretation for the proximity effect along the line of sights. While, the illumination from quasars along the transverse directions would much less than that along the sightlines of quasars (e.g., Jalan et al. 2019), so there is an inverse proximity effect along the transverse directions (commonly called as transverse proximity effect).

In order to check the influence on the incident rate of Mg II absorption lines from quasar radiation, we compare the incident rates of Mg II absorption lines between the subsamples whose foreground quasars host different luminosities. The results are displayed in Figure 7 as

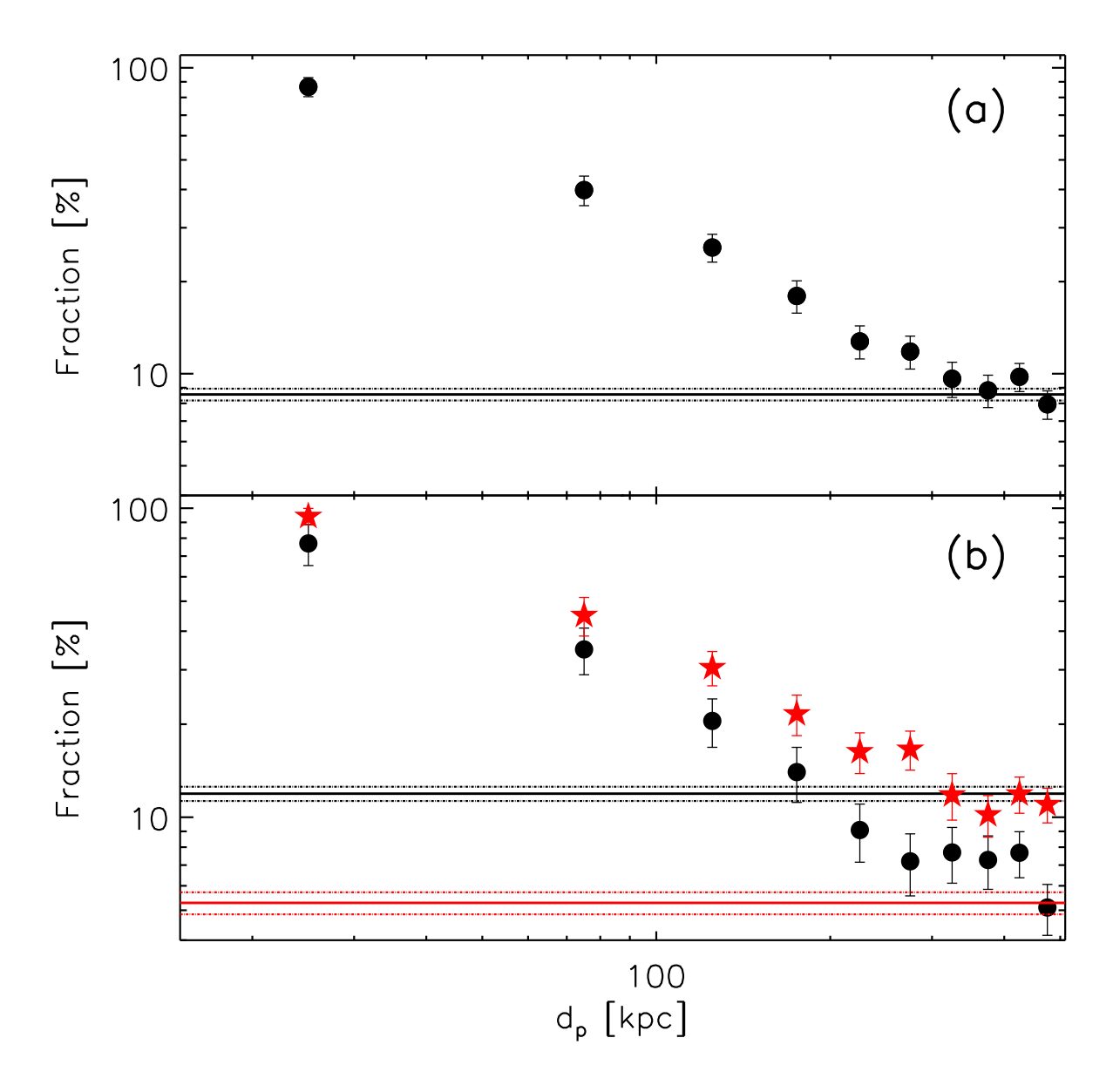


Figure 7. The incident rate of detected TRA Mg II absorption lines as a function of projected distance. Horizontal solid lines represent incident rates of detected LOS Mg II absorption lines, and dot-dash lines represent $\pm 1\sigma$ error of the incident rates of detected LOS Mg II absorption lines. Note that these fractions for the LOS Mg II are averaged over the entire velocity bin considered. Panel (a) is for all the quasar pairs, where $f_c = 8.554 \pm 0.381\%$ for the LOS Mg II absorption lines. Panel (b): Black symbols (circles and horizonal lines) are for the quasar pairs whose foreground quasars have $LogL_{bol} \leq 45.66$ erg s⁻¹, and the red symbols (stars and horizonal lines) are for the quasar pairs whose foreground quasars have $LogL_{bol} > 45.66$ erg s⁻¹. For the LOS Mg II absorption lines, faint foreground quasars have $f_c = 11.919 \pm 0.633\%$, and luminous quasars have $f_c = 5.283 \pm 0.433\%$.

well. It is clearly seen that the quasars with higher luminosities (red lines in panel (b) of Figure 7) have an obviously ($> 5\sigma$) smaller incidence of LOS Mg II absorption lines, when compared to the quasars with lower luminosities (black lines in panel (b) of Figure 7). This difference would be the expectation of the proximity effect along quasar sightline, since the quasars with higher luminosities evaporate more Mg II absorbing gas close to quasars, when compared to the quasars with lower

luminosities. While along the transverse direction, it can be clearly seen from Figure 7 that the incident rate of TRA Mg II absorption lines is higher for more luminous quasars (red stars in panel (b) of Figure 7). It is believe that only a small portion of quasar's illumination pass through the gas clouds along transverse direction. Therefore for the more luminous quasars, not only the Mg II absorbing gas is not evaporated but also more neutral magnesium is ionized into ionic gas. This leads

Table 4.	The incident	rate of TRA	Mg II	absorption lin	es
----------	--------------	-------------	-------	----------------	----

$d_p \mathrm{bin} (\mathrm{kpc})$	$f_{ m c}$
(0,50]	86.7 ± 6.2
(50,100]	$39.8 {\pm} 4.4$
(100,150]	$25.9 {\pm} 2.7$
(150,200]	17.9 ± 2.2
(200,250]	$12.8 {\pm} 1.6$
(250,300]	11.8 ± 1.5
(300, 350]	9.6 ± 1.3
(350,400]	8.8 ± 1.1
(400, 450]	9.8 ± 1.0
(450,500]	7.9 ± 0.8

to a greater incident rate of TRA Mg II absorption lines for the more luminous quasars. Of course, these discrepancies could be also related to a bias in the quasar host properties. For instance, the bright quasars would be expected to host halos with masses larger than those of faint quasars, which could also affect in the gas distribution.

7. SUMMARY

We have constructed a large sample of 10025 quasar pairs with $d_{\rm p} < 500$ kpc from the final data set of the SDSS-IV, to analyze the properties of Mg II absorption lines around foreground quasars, including both the LOS and TRA absorptions. We find that there are 598 background quasars with detected TRA Mg II absorption lines, and 454 foreground quasars with detected LOS Mg II absorption lines.

The velocity dispersion (σ , line width) of all the TRA Mg II absorption lines is less than 250 km s⁻¹. The line width of LOS Mg II absorption lines have a value of σ < 300 km s⁻¹, except for 4 systems with 300 < σ < 400 km s⁻¹. Both the LOS and TRA Mg II absorption lines are mainly constrained within a velocity dispersion of

 $60 < \sigma < 150 \text{ km s}^{-1}$. Meanwhile, for a vast majority of both the TRA and LOS Mg II absorption lines, the relative velocity of absorption lines (v_r , with respect to foreground quasar systemic redshift) is within a range of $|v_r| < 600 \text{ km s}^{-1}$. Combining the small/mild velocity dispersion and small relative velocity, most of the TRA and LOS Mg II absorption lines would be dominated by the gas medium gravitationally bounded by quasar halo.

Both the equivalent width and incident rate of TRA Mg II absorption lines are rapidly decreased with increasing distance. The incident rate of TRA Mg II absorption lines is obviously (> 4σ) greater than that of LOS Mg II absorption lines at projected distances $d_p < 200$ kpc, and they become consistent within 3σ at $d_p > 200$ kpc. The anisotropic radiation from quasars would be the most possible interpretation for the anisotropic absorption around quasars. The powerful outflow/jet likely over ionizes the gas medium with low ionization state along quasar sightlines, and impose a so-called proximity effect that obviously reduces the incidence of absorptions along quasar sightlines. While along the transverse direction, the less illumination from quasars can not drive a transverse proximity effect. The TRA and LOS Mg II absorption lines both have similar incidences at $d_p > 200$ kpc, which hints that the quasar feedback from powerful outflows/jets is not significantly influencing the Mg II gas around quasars on large scales. Of course, the scale of quasar feedback would be related to quasar's luminosity or accretion rate.

ACKNOWLEDGEMENTS

We deeply thank the anonymous referees for her/his helpful and careful comments. This work is supported by the National Natural Science Foundation of China (12073007), the Guangxi Natural Science Foundation (2019GXNSFFA245008; GKAD19245136), and the Scientific Research Project of Guangxi University for Nationalities (2018KJQD01).

REFERENCES

Abazajian, K. N., Adelman-McCarthy, J. K., Agüeros, M. A., et al. 2009, ApJS, 182, 543, doi: 10.1088/0067-0049/182/2/543

Almeyda, T., Robinson, A., Richmond, M., Vazquez, B., & Nikutta, R. 2017, ApJ, 843, 3,

doi: 10.3847/1538-4357/aa7687

Anand, A., Nelson, D., & Kauffmann, G. 2021, MNRAS, 504, 65, doi: 10.1093/mnras/stab871

Antonucci, R. 1993, ARA&A, 31, 473,

doi: 10.1146/annurev.aa.31.090193.002353

Arrigoni Battaia, F., Hennawi, J. F., Prochaska, J. X., et al. 2019, MNRAS, 482, 3162, doi: 10.1093/mnras/sty2827
Arrigoni Battaia, F., Prochaska, J. X., Hennawi, J. F., et al.

2018, MNRAS, 473, 3907, doi: 10.1093/mnras/stx2465 Bahcall, J. N. 1978, PhyS, 17, 229,

doi: 10.1088/0031-8949/17/3/016

Bahcall, J. N., & Salpeter, E. E. 1966, ApJ, 144, 847, doi: 10.1086/148675

Bahcall, J. N., & Spitzer, Lyman, J. 1969, ApJL, 156, L63, doi: 10.1086/180350

- Barnes, L. A., Garel, T., & Kacprzak, G. G. 2014, PASP, 126, 969, doi: 10.1086/679178
- Barrera-Ballesteros, J. K., Falcón-Barroso, J., García-Lorenzo, B., et al. 2014, A&A, 568, A70, doi: 10.1051/0004-6361/201423488
- Bielby, R. M., Fumagalli, M., Fossati, M., et al. 2020, MNRAS, 493, 5336, doi: 10.1093/mnras/staa546
- Bordoloi, R., Lilly, S. J., Knobel, C., et al. 2011, ApJ, 743, 10, doi: 10.1088/0004-637X/743/1/10
- Borisova, E., Cantalupo, S., Lilly, S. J., et al. 2016, ApJ, 831, 39, doi: 10.3847/0004-637X/831/1/39
- Bowen, D. V., Hennawi, J. F., Ménard, B., et al. 2006, ApJL, 645, L105, doi: 10.1086/506274
- Burbidge, G., O'Dell, S. L., Roberts, D. H., & Smith, H. E. 1977, ApJ, 218, 33, doi: 10.1086/155654
- Burchett, J. N., Rubin, K. H. R., Prochaska, J. X., et al. 2021, ApJ, 909, 151, doi: 10.3847/1538-4357/abd4e0
- Cai, Z., Cantalupo, S., Prochaska, J. X., et al. 2019, ApJS, 245, 23, doi: 10.3847/1538-4365/ab4796
- Cantalupo, S., Arrigoni-Battaia, F., Prochaska, J. X., Hennawi, J. F., & Madau, P. 2014, Nature, 506, 63, doi: 10.1038/nature12898
- Cantalupo, S., Pezzulli, G., Lilly, S. J., et al. 2019, MNRAS, 483, 5188, doi: 10.1093/mnras/sty3481
- Carswell, R. F., Whelan, J. A. J., Smith, M. G., Boksenberg, A., & Tytler, D. 1982, MNRAS, 198, 91, doi: 10.1093/mnras/198.1.91
- Chen, H.-W., Helsby, J. E., Gauthier, J.-R., et al. 2010a, ApJ, 714, 1521, doi: 10.1088/0004-637X/714/2/1521
- Chen, H.-W., & Tinker, J. L. 2008, ApJ, 687, 745, doi: 10.1086/591927
- Chen, H.-W., Wild, V., Tinker, J. L., et al. 2010b, ApJL, 724, L176, doi: 10.1088/2041-8205/724/2/L176
- Chen, Z., He, Z., Ho, L. C., et al. 2022a, Nature Astronomy, 6, 339, doi: 10.1038/s41550-021-01561-3
- Chen, Z.-F. 2013, Research in Astronomy and Astrophysics, 13, 641, doi: 10.1088/1674-4527/13/6/001
- Chen, Z.-F., Gu, M., He, Z., et al. 2022b, A&A, 659, A103, doi: 10.1051/0004-6361/202142307
- Chen, Z.-F., Gu, Q.-S., & Chen, Y.-M. 2015, ApJS, 221, 32, doi: 10.1088/0067-0049/221/2/32
- Chen, Z.-F., Gu, Q.-S., Zhou, L., & Chen, Y.-M. 2016, MNRAS, 462, 2980, doi: 10.1093/mnras/stw1872
- Chen, Z.-F., Huang, W.-R., Pang, T.-T., et al. 2018a, ApJS, 235, 11, doi: 10.3847/1538-4365/aaaaec
- Chen, Z.-F., & Pan, D.-S. 2017, ApJ, 848, 79, doi: 10.3847/1538-4357/aa8d66
- Chen, Z.-F., Qin, H.-C., Gui, R.-J., et al. 2020, ApJS, 250, 3, doi: 10.3847/1538-4365/aba520

- Chen, Z.-F., Yi, S.-X., Pang, T.-T., et al. 2019, ApJS, 244, 36, doi: 10.3847/1538-4365/ab41fe
- Chen, Z.-F., Yao, M., Pang, T.-T., et al. 2018b, ApJS, 239, 23, doi: 10.3847/1538-4365/aaeac3
- Churchill, C. W., Nielsen, N. M., Kacprzak, G. G., & Trujillo-Gomez, S. 2013, ApJL, 763, L42, doi: 10.1088/2041-8205/763/2/L42
- Cooksey, K. L., Kao, M. M., Simcoe, R. A., O'Meara, J. M., & Prochaska, J. X. 2013, ApJ, 763, 37, doi: 10.1088/0004-637X/763/1/37
- Cunnama, D., Andrianomena, S., Cress, C. M., et al. 2014, MNRAS, 438, 2530, doi: 10.1093/mnras/stt2380
- Dawson, K. S., Schlegel, D. J., Ahn, C. P., et al. 2013, AJ, 145, 10, doi: 10.1088/0004-6256/145/1/10
- Dawson, K. S., Kneib, J.-P., Percival, W. J., et al. 2016, AJ, 151, 44, doi: 10.3847/0004-6256/151/2/44
- DeFelippis, D., Bouché, N. F., Genel, S., et al. 2021, ApJ, 923, 56, doi: 10.3847/1538-4357/ac2cbf
- Drake, A. B., Farina, E. P., Neeleman, M., et al. 2019, ApJ, 881, 131, doi: 10.3847/1538-4357/ab2984
- Dutta, R., Fumagalli, M., Fossati, M., et al. 2020, MNRAS, 499, 5022, doi: 10.1093/mnras/staa3147
- Elvis, M. 2000, ApJ, 545, 63, doi: 10.1086/317778
- Farina, E. P., Falomo, R., Decarli, R., Treves, A., & Kotilainen, J. K. 2013, MNRAS, 429, 1267, doi: 10.1093/mnras/sts410
- Farina, E. P., Falomo, R., Scarpa, R., et al. 2014, MNRAS, 441, 886, doi: 10.1093/mnras/stu585
- Farina, E. P., Venemans, B. P., Decarli, R., et al. 2017, ApJ, 848, 78, doi: 10.3847/1538-4357/aa8df4
- Farina, E. P., Arrigoni-Battaia, F., Costa, T., et al. 2019, ApJ, 887, 196, doi: 10.3847/1538-4357/ab5847
- Fossati, M., Fumagalli, M., Lofthouse, E. K., et al. 2019, MNRAS, 490, 1451, doi: 10.1093/mnras/stz2693
- —. 2021, MNRAS, 503, 3044, doi: 10.1093/mnras/stab660
- Ginolfi, M., Maiolino, R., Carniani, S., et al. 2018, MNRAS, 476, 2421, doi: 10.1093/mnras/sty364
- Gunn, J. E., Siegmund, W. A., Mannery, E. J., et al. 2006, AJ, 131, 2332, doi: 10.1086/500975
- Guo, Y., Maiolino, R., Jiang, L., et al. 2020, ApJ, 898, 26, doi: 10.3847/1538-4357/ab9b7f
- He, Z., Wang, T., Zhou, H., et al. 2017, ApJS, 229, 22, doi: 10.3847/1538-4365/aa647a
- He, Z., Liu, G., Wang, T., et al. 2022, Science Advances, 8, eabk3291, doi: 10.1126/sciadv.abk3291
- Hennawi, J. F., & Prochaska, J. X. 2007, ApJ, 655, 735, doi: 10.1086/509770
- —. 2013, ApJ, 766, 58, doi: 10.1088/0004-637X/766/1/58

- Hennawi, J. F., Prochaska, J. X., Cantalupo, S., & Arrigoni-Battaia, F. 2015, Science, 348, 779, doi: 10.1126/science.aaa5397
- Hennawi, J. F., Prochaska, J. X., Burles, S., et al. 2006, ApJ, 651, 61, doi: 10.1086/507069
- Hewett, P. C., & Wild, V. 2010, MNRAS, 405, 2302, doi: 10.1111/j.1365-2966.2010.16648.x
- Ho, S. H., Martin, C. L., & Schaye, J. 2020, ApJ, 904, 76, doi: 10.3847/1538-4357/abbe88
- Huang, Y.-H., Chen, H.-W., Johnson, S. D., & Weiner, B. J. 2016, MNRAS, 455, 1713, doi: 10.1093/mnras/stv2327
- Huang, Y.-H., Chen, H.-W., Shectman, S. A., et al. 2021, MNRAS, 502, 4743, doi: 10.1093/mnras/stab360
- Jalan, P., Chand, H., & Srianand, R. 2019, ApJ, 884, 151, doi: 10.3847/1538-4357/ab4191
- Jin, G., Dai, Y. S., Pan, H.-A., et al. 2021, ApJ, 923, 6, doi: 10.3847/1538-4357/ac2901
- Johnson, S. D., Chen, H.-W., & Mulchaey, J. S. 2015, MNRAS, 452, 2553, doi: 10.1093/mnras/stv1481
- Joshi, R., Srianand, R., Petitjean, P., & Noterdaeme, P. 2018, MNRAS, 476, 210, doi: 10.1093/mnras/sty121
- Kacprzak, G. G., Churchill, C. W., Evans, J. L., Murphy, M. T., & Steidel, C. C. 2011, MNRAS, 416, 3118, doi: 10.1111/j.1365-2966.2011.19261.x
- Kacprzak, G. G., Churchill, C. W., Murphy, M. T., & Cooke, J. 2015, MNRAS, 446, 2861, doi: 10.1093/mnras/stu2324
- Kacprzak, G. G., Churchill, C. W., Steidel, C. C., Murphy,M. T., & Evans, J. L. 2007, ApJ, 662, 909,doi: 10.1086/517990
- Lan, T.-W., & Mo, H. 2018, ApJ, 866, 36, doi: 10.3847/1538-4357/aadc08
- Landoni, M., Falomo, R., Treves, A., Scarpa, R., & Farina, E. P. 2016, MNRAS, 457, 267, doi: 10.1093/mnras/stv2964
- Lau, M. W., Prochaska, J. X., & Hennawi, J. F. 2016, ApJS, 226, 25, doi: 10.3847/0067-0049/226/2/25
- —. 2018, ApJ, 857, 126, doi: 10.3847/1538-4357/aab78e
- Law, D. R., Yan, R., Bershady, M. A., et al. 2015, AJ, 150, 19, doi: 10.1088/0004-6256/150/1/19
- Lee, J. C., Hwang, H. S., & Song, H. 2021, MNRAS, 503, 4309, doi: 10.1093/mnras/stab637
- Lofthouse, E. K., Fumagalli, M., Fossati, M., et al. 2022, arXiv e-prints, arXiv:2209.15021. https://arxiv.org/abs/2209.15021
- Lovegrove, E., & Simcoe, R. A. 2011, ApJ, 740, 30, doi: 10.1088/0004-637X/740/1/30
- Lyke, B. W., Higley, A. N., McLane, J. N., et al. 2020, ApJS, 250, 8, doi: 10.3847/1538-4365/aba623

- Madau, P., & Dickinson, M. 2014, ARA&A, 52, 415, doi: 10.1146/annurev-astro-081811-125615
- Martin, D. C., Chang, D., Matuszewski, M., et al. 2014, ApJ, 786, 106, doi: 10.1088/0004-637X/786/2/106
- Martin, D. C., Matuszewski, M., Morrissey, P., et al. 2015, Nature, 524, 192, doi: 10.1038/nature14616
- Matejek, M. S., & Simcoe, R. A. 2012, ApJ, 761, 112, doi: 10.1088/0004-637X/761/2/112
- Ménard, B., Wild, V., Nestor, D., et al. 2011, MNRAS, 417, 801, doi: 10.1111/j.1365-2966.2011.18227.x
- Muzahid, S., Schaye, J., Cantalupo, S., et al. 2021, MNRAS, 508, 5612, doi: 10.1093/mnras/stab2933
- Nestor, D. B., Johnson, B. D., Wild, V., et al. 2011, MNRAS, 412, 1559,
 - doi: 10.1111/j.1365-2966.2010.17865.x
- Nielsen, N. M., Kacprzak, G. G., Pointon, S. K., et al. 2020, ApJ, 904, 164, doi: 10.3847/1538-4357/abc561
- Nielsen, N. M., Kacprzak, G. G., Sameer, et al. 2022, MNRAS, 514, 6074, doi: 10.1093/mnras/stac1824
- Opher, R. 1974, Nature, 250, 310, doi: 10.1038/250310a0
- O'Sullivan, D. B., Martin, C., Matuszewski, M., et al. 2020, ApJ, 894, 3, doi: 10.3847/1538-4357/ab838c
- Prochaska, J. X., Hennawi, J. F., & Simcoe, R. A. 2013a, ApJL, 762, L19, doi: 10.1088/2041-8205/762/2/L19
- Prochaska, J. X., Lau, M. W., & Hennawi, J. F. 2014, ApJ, 796, 140, doi: 10.1088/0004-637X/796/2/140
- Prochaska, J. X., Hennawi, J. F., Lee, K.-G., et al. 2013b, ApJ, 776, 136, doi: 10.1088/0004-637X/776/2/136
- Prochter, G. E., Prochaska, J. X., & Burles, S. M. 2006, ApJ, 639, 766, doi: 10.1086/499341
- Roeser, H. J. 1975, A&A, 45, 329
- Sandrinelli, A., Falomo, R., Treves, A., Farina, E. P., & Uslenghi, M. 2014, MNRAS, 444, 1835, doi: 10.1093/mnras/stu1526
- Shen, Y. 2016, ApJ, 817, 55, doi: 10.3847/0004-637X/817/1/55
- Shen, Y., & Ménard, B. 2012, ApJ, 748, 131, doi: 10.1088/0004-637X/748/2/131
- Shen, Y., Richards, G. T., Strauss, M. A., et al. 2011, ApJS, 194, 45, doi: 10.1088/0067-0049/194/2/45
- Smee, S. A., Gunn, J. E., Uomoto, A., et al. 2013, AJ, 146, 32, doi: 10.1088/0004-6256/146/2/32
- Srianand, R., & Khare, P. 1996, MNRAS, 280, 767, doi: 10.1093/mnras/280.3.767
- Steidel, C. C., Erb, D. K., Shapley, A. E., et al. 2010, ApJ, 717, 289, doi: 10.1088/0004-637X/717/1/289
- Tinker, J. L., & Chen, H.-W. 2008, ApJ, 679, 1218, doi: 10.1086/587432

- Tumlinson, J., Peeples, M. S., & Werk, J. K. 2017, ARA&A, 55, 389,
 - doi: 10.1146/annurev-astro-091916-055240
- Tytler, D., Gleed, M., Melis, C., et al. 2009, MNRAS, 392, 1539, doi: 10.1111/j.1365-2966.2008.14159.x
- Wild, V., Kauffmann, G., White, S., et al. 2008, MNRAS, 388, 227, doi: 10.1111/j.1365-2966.2008.13375.x
- York, D. G., Adelman, J., Anderson, John E., J., et al. 2000, AJ, 120, 1579, doi: 10.1086/301513
- Zhou, Y., Chen, Y., Shi, Y., et al. 2022, MNRAS, doi: 10.1093/mnras/stac2016

- Zhu, G., & Ménard, B. 2013, ApJ, 770, 130, doi: 10.1088/0004-637X/770/2/130
- Zhu, G., Ménard, B., Bizyaev, D., et al. 2014, Monthly Notices of the Royal Astronomical Society, 439, 3139, doi: 10.1093/mnras/stu186
- Zhu, Y., Bu, D.-F., Yang, X.-H., Yuan, F., & Lin, W.-B.
 2022, MNRAS, 513, 1141, doi: 10.1093/mnras/stac1015